Chemistry–A European Journal | Research Article
doi.org/10.1002/chem.202202006
Chemistry Europe
European Chemical Societies Publishing
www.chemeurj.org

Biocatalytic Intramolecular C–H aminations via Engineered Heme Proteins: Full Reaction Pathways and Axial Ligand Effects

Yang Wei,[a, b] Melissa Conklin,[a] and Yong Zhang*[a]

Abstract: Engineered heme protein biocatalysts provide an efficient and sustainable approach to develop amine-containing compounds through C–H amination. A quantum chemical study to reveal the complete heme catalyzed intramolecular C–H amination pathway and protein axial ligand effect was reported, using reactions of an experimentally used arylsulfonylazide with hemes containing L = none, SH^-, MeO^-, and MeOH to simulate no axial ligand, negatively charged Cys and Ser ligands, and a neutral ligand for comparison. Nitrene formation was found as the overall rate-determining step (RDS) and the catalyst with Ser ligand has the best reactivity, consistent with experimental reports. Both RDS and non-RDS (nitrene transfer) transition states follow the barrier trend of $MeO^- < SH^- <$ MeOH < None due to the charge donation capability of the axial ligand to influence the key charge transfer process as the electronic driving forces. Results also provide new ideas for future biocatalyst design with enhanced reactivities.

Introduction

Because of functionalities in both natural products and therapeutic drugs,[1] the development of catalysts for the amination of $C(sp^3)$–H bonds has attracted much attention and been widely applied in organic synthesis.[2] These reactions require catalysts that are often expensive, as well as nitrene sources that are potentially harmful to the environment.[3] Cost-effective, green synthesis of these amine-containing compounds would therefore be a potent tool in this field. Due to high reactivity and enantioselectivity of metalloporphyrin catalysts,[4] major efforts have been exerted on exploring metalloporphyrins and more recently engineered heme proteins in catalytic C–H aminations, including metal centers such as Fe,[5] Co,[6] and Ru.[7] Among available nitrene sources, organic azides are environmentally friendly (which upon reaction with heme catalysts generate the harmless gas N_2 as the sole byproduct[6b,8]), highly reactive,[8–9] and easily accessible.[9b,c] Recent experimental studies show that engineered heme proteins[5,10] can promote the C–H amination transformation of azide substrates at room temperature with up to 14000 turnovers and up to >99% ee.[5h,j] Such favorable catalytic features coupled with the facts that Fe is the most abundant and least expensive transition metal and heme proteins are not toxic, make these biocatalysts highly appealing for sustainable chemical synthesis.

In contrast, the theoretical mechanistic work of heme protein catalyzed C–H amination is scarce,[5j,11] although there are a few reports of metalloporphyrin catalyzed C–H amination mechanisms.[6a,c,e,f,12] In particular, there is only one computational report for the intramolecular C–H aminations catalyzed by heme proteins,[11c] which is focused on explaining regio- and stereo-selectivity. But the whole intramolecular C–H amination pathway starting from reactants is unknown, which is important for the information of the overall rate-determining step (RDS) and biocatalyst design. Moreover, there are other interesting mechanistic questions unaddressed for many experimental intramolecular C–H amination studies.[5a–e,g,h] For instance, Arnold[5a] and Fasan[5h] groups revealed a significant intramolecular C–H amination reactivity improvement by just mutating the axial Cys ligand to Ser in native cytochrome P450 variants. This beneficial mutation was then included in many intra- and even intermolecular C–H amination experimental work.[5a,d,f–j] However, the mechanistic origin of this favorable axial ligand effect has not been well understood yet. Although a very recent computational work on the intermolecular heme C–H amination studied these two ligands,[11d] the comparison is only on the nitrene formation process (this step was determined to be not a RDS there, which is inconsistent with other recent computational reports on the same reaction[11a,b]) and prefers the protonated Ser over the deprotonated one, which is also inconsistent with all other computational work in this field.[5j,11a–c] These problems call for a more careful and complete reaction pathway study of the effects of Cys vs. protonated and

[a] Dr. Y. Wei, M. Conklin, Prof. Dr. Y. Zhang
Department of Chemistry and Chemical Biology
Stevens Institute of Technology
1 Castle Point on Hudson, Hoboken, NJ 07030 (USA)
E-mail: yong.zhang@stevens.edu

[b] Dr. Y. Wei
Department of Chemistry and Biochemistry
Loyola University Chicago
1032 W Sheridan Rd, Chicago, IL 60660 (USA)

Supporting information for this article is available on the WWW under https://doi.org/10.1002/chem.202202006

deprotonated Ser. In addition, The mechanistic comparison with no ligand is still unknown.

As such, we report the results of full intramolecular C–H amination pathway and axial ligand effect via a quantum chemical study of heme catalyzed intramolecular C–H aminations of arylsulfonyl azide. These data not only well reproduced available experimental reactivity trend of axial ligands and RDS[5a,h] and other features from prior experimental and computational work,[11a–c,13] but more importantly revealed the previously unknown electronic driving forces for the key transition states and electronic origin of the observed ligand effect. Such information will benefit future biocatalyst design for C–H aminations. This work also enriches the mechanistic understanding of axial ligand effects on various kinds of heme reactions[13a,14] and the chemistry of P450s.[5j,11,13a,14a–c,e,g,i,15]

Results and Discussion

Since we focus on the axial ligand effect and basic full reaction pathway, the heme catalysts ($\mathbf{R_1}$) with different axial ligand situations were modeled as [Fe(Por)L] (L = none for no axial ligand, SH^- for Cys,[13a,14b] OMe^- for Ser,[5j,11a–c] and MeOH for a neutral ligand; Por = non-substituted porphyrin, as used in recent computational studies of C–H aminations[5j,11b–d]). The substrate is the experimentally used 2,4,6-triethylbenzene-1-sulfonylazide ($\mathbf{R_2}$).[5a–c,e] As shown in the Supporting Information, additional calculations using the full heme substituents in the real proteins show that all conclusions including the rate-determining step, the more favorable reactivity of Ser vs. Cys, and spin state effects remain the same, thus support the efficient use of the current models in this work for subsequent discussion. All species in the reaction pathways were subject to full geometry optimizations and frequency analysis using a range-separated hybrid DFT method with dispersion correction based on its excellent performance for heme carbene reaction pathway studies.[13,14b,d,16]

Because conformation may influence the reaction results,[13b,14b,d] we first conducted a detailed study of possible conformations of the substrate, and then study species in the reaction pathway involving both the substrate and heme catalyst, to choose the most reasonable conformations in the following mechanistic investigation, see section I in Supporting Information for details.

In addition, because the studied iron-containing systems could have different spin states and various spin interactions among different components in each system, we carried out a comprehensive spin state study (see details in section II of Supporting Information) to use the most favorable spin state for each system in the subsequent mechanistic discussion.

Full intramolecular C-H amination pathway and RDS

As shown in Figure 1, the basic reaction pathway is similar to previous work of metalloporphyrin-catalyzed C–H aminations,[6a,11b,c,12a] having first nitrene formation and then

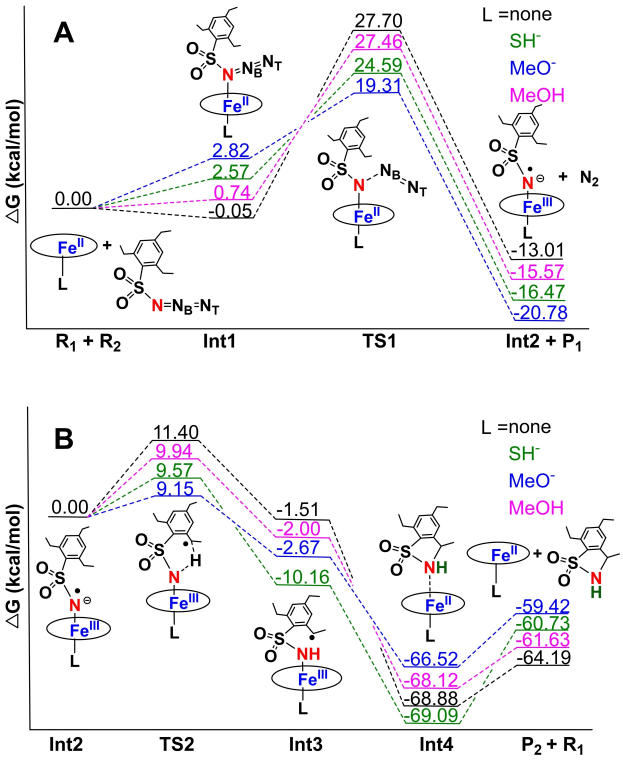

Figure 1. Relative Gibbs free energy profiles with different axial ligands for species in the reaction pathways of (**A**) nitrene formation and (**B**) C–H amination.

nitrene transfer (C–H amination) steps. It should be noted that the general reaction pathway feature described here is the same no matter there is no ligand, negatively charged ligands with different coordination atoms, or neutral ligand. The reaction starts with $\mathbf{R_2}$ coordination to $\mathbf{R_1}$ to form the first intermediate (**Int1**), which only has a mild energy cost due to entropic effect (the enthalpy is favorable for this step, see Table S10). Then, it proceeds through the first transition state (**TS1**) for the formation of the nitrenoid intermediate (**Int2**) with release of N_2 ($\mathbf{P_1}$). **TS1** has a significant barrier (> 19 kcal/mol) and is the RDS in the whole reaction pathway for all ligand cases (see Figure 1A vs. 1B). This feature agrees with a recent experimental work of heme protein catalyzed intramolecular C–H aminations.[5h] Subsequently, a benzylic hydrogen atom is transferred to the nitrene nitrogen via the second transition state (**TS2**) to generate the third intermediate (**Int3**). The reaction barrier in this step is around 10 kcal/mol. Then, the nitrene nitrogen bonds with the radical benzylic carbon to form the fourth intermediate (**Int4**). All efforts in trying to obtain a radical rebound transition state connecting **Int3** and **Int4** failed, which suggests a barrierless process for this step and is probably due to the strong thermodynamic favorability of this reaction step with > ~60 kcal/mol energy drop. The absence of this transition state was also reported in some heme catalyzed intermolecular C–H amination pathways.[11a,b] Finally, the breaking of the Fe–N coordination bond in **Int4** delivers the C–H amination product ($\mathbf{P_2}$) and regenerates the catalyst $\mathbf{R_1}$. Overall,

these results provide the first intramolecular C–H amination pathways and show that nitrene formation is the overall RDS in this multiple step reaction.

Axial ligand effect

We then investigate the details of axial ligand effects on catalytic reactivities, which exhibit a range of ~8 kcal/mol for **TS1** barriers in contrast with only ~2 kcal/mol differences in **TS2** barriers, see Figure 1. This again highlights the importance of **TS1**, which as RDS is more sensitive to catalyst structural changes. Based on RDS barriers, the Cys axial ligand is significantly less favorable than the Ser ligand in promoting nitrene formation, which is in good accordance with experimental observations.[5a,h] The correct identification of experimentally proved RDS and axial ligand effect shows further support of using these computational results to understand some mechanistic features unknown before. Interestingly, for RDS, the barriers for a neutral ligand and no ligand (also a neutral axial environment) are very similar (< 1 kcal/mol difference) and both are much higher than those for the two negatively charged ligand cases. In particular, the significantly more favorable barrier for MeO^- than that for MeOH with the same coordination atom and substituent and the only difference of the charge state, is a strong indicator of the electronic effect of the axial ligand's charge. Even for non-RDS **TS2** barriers, Ser is more favorable than Cys as the axial ligand and both are again lower than the cases of neutral axial environments. So, these computational results provide several interesting reactivity trends as regards axial ligand or ligand environment and suggest that the charge state of an axial ligand is important for both nitrene formation and transfer reactions.

Based on this complete reaction pathway study, the deprotonated Ser is preferred over the protonated one for this reaction and only the deprotonated Ser reproduces the experimental reactivity trend of Ser > Cys.[5a,h] The use of deprotonated Ser is consistent with all computational work in heme C–H amination studies[5j,11a–c] except for one recent paper which was based on a comparison of only the nitrene formation step (determined to be non-RDS there,[11d] which is inconsistent with other recent computational reports on the same reaction[11a,b]) for protonated Ser and deprotonated Cys. That work used absolute deprotonation energies calculated from two processes that have not been proved to be experimentally applicable for its protonation state. In contrast, a recent computational work of heme carbene transfer reactions which employed relative deprotonation energies compared to a species that is known to be deprotonated in the neutral pH range showed that both Ser and Cys shall be deprotonated.[14a] Such deprotonated Ser was also used in other computational heme carbene reaction studies.[14c] In addition, experimental x-ray structures of Cys to Ser mutated P450s (called P411s)[5f,17] show that the same hydrogen bonding partners to stabilize the deprotonated Cys in the native enzyme are maintained during the mutation to Ser, which also suggests a similar stabilization effect for the deprotonated Ser.

Nitrene formation step

To help understand origin of these reactivity differences of various ligand situations, both charge profiles and geometric data were examined in detail (see Tables S11 and S12) with key results shown in Figures 2 and 3 respectively. The charge distribution in the reaction system varies along the pathway to result in charge transfer (CT) from some parts to other parts of the system. Analysis of this kind of results have assisted the elucidation of electronic effects and particularly the electronic driving forces of other reactions for heme systems.[13b,14b,d] As shown in Figure 2A–D, there is a significant CT occurs from Fe to the coordinated azide group from reactants to **TS1** for all four ligand cases. It has a value around 0.6 e, which indicates the partial formation of Fe(III) and negatively charged nitrene moiety at **TS1**. This electron transfer feature is more evident from the spin density analysis, showing a total spin density of ca. 1 e for the N_3 group and corresponding spin density for an Fe(III) center (see Table S13). The major energy cost in this stage is the partial cleavage of the $N\text{-}N_B$ bond to prepare for the N_2 release. This is associated with ca. 0.4 Å bond elongation (which is much larger than other bond length changes around the reaction center, see Table 1) and ca. 50 degrees of bending for the $N\text{-}N_B\text{-}N_T$ angle, see Figure 3A–D. Because the $N\text{-}N_B$ bond in the original azide has a positive charge of ~0.3 e (Table S12), a negative CT of this amount to this moiety (Q_{CT1}) happens for releasing a neutral N_2, see Figure 2A–D. This CT accounts for

Table 1. Key Energetic, Geometric, and Electronic Results.

L	[a]	$\Delta G^{\ddagger}$ [kcal/mol]	$R_{Fe\text{-}N}$ [Å]	$\Delta R_{N\text{-}NB}$ [Å]	$\Delta R_{C\text{-}H}$ [Å]	Q_{CT} [b] [e]	$\rho^{\alpha\beta}{}_{Fe}$ [e]	$\rho^{\alpha\beta}{}_{N}$ [e]	$\rho^{\alpha\beta}{}_{C}$ [e]
MeO^-	^{3}**TS1**	19.31	2.073	0.375	−0.002	−0.327	0.950	0.401	0.001
	^{3}**TS2**	9.15	1.983		0.204	−0.202	0.918	0.526	0.525
SH^-	^{3}**TS1**	24.59	2.049	0.370	−0.002	−0.322	1.096	0.398	0.001
	^{3}**TS2**	9.57	1.938		0.193	−0.203	1.025	0.534	0.515
MeOH	^{5}**TS1**	27.46	2.148	0.385	−0.001	−0.311	2.851	0.549	0.002
	^{3}**TS2**	9.94	1.835		0.176	−0.218	0.977	0.576	0.499
none	^{5}**TS1**	27.70	2.092	0.379	−0.001	−0.302	2.779	0.568	0.000
	^{3}**TS2**	11.40	1.810		0.178	−0.239	1.041	0.520	0.498

a) Corresponding spin states of the transition states are indicated by the left superscript. b) the major CT responsible for the energy barrier as described in the text: Q_{CT1} for **TS1** and Q_{CT2} for **TS2**.

Research Article
doi.org/10.1002/chem.202202006

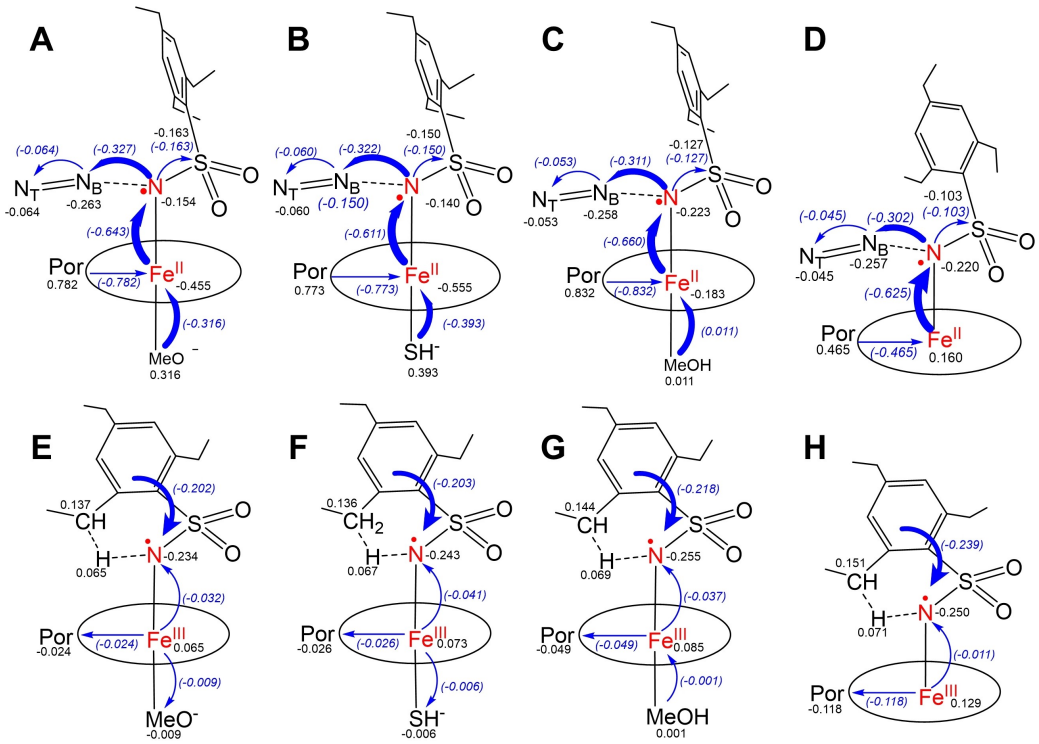

Figure 2. Atomic charge changes (in black) at **TS1** (**A**–**D**) with respect to reactants and **TS2** (**E**–**H**) with respect to **Int2** and charge transfers (in blue) as indicated by arrows and numbers in parentheses for the four axial ligand cases.

~50% of the total charge received from Fe or heme to azide, with the remaining ~30% and 20% located at the nitrene's nitrogen and further transferred to the arylsulfonyl part respectively. It is interesting to note that $|Q_{CT1}|$ follows a trend of $MeO^- > SH^- > MeOH >$ None, i.e. the larger the CT (in magnitude, all being negative CTs), the lower the barrier, and the greater the reactivity for **TS1** with respect to reactants. These results show that the CT from Fe to azide and eventually to the terminal N_2 moiety is a significant change and Q_{CT1} at **TS1** for breaking the N-N_B bond is correlated with the reaction barrier. Based on this electronic driving force, an axial ligand can significantly influence the reactivity via its charge donation capability. This feature helps understand the more favorable reactivity of a negatively charged axial ligand than a neutral ligand discussed above, since a negatively charged ligand can donate more charge to Fe to facilitate the CT process needed for bond-breaking at **TS1**. Among the two negatively charged ligands studied here, the Fe–O bond is ca. 0.5 Å shorter than the Fe–S bond (see Figure 3A–B), which aids the charge donation from Fe to azide (see Figure 2A–B) to eventually release the charge to N_2 moiety for its leaving. This leads to a smaller barrier for MeO^- than SH^-.

It is interesting to note that the axial ligand effect regarding a neutral ligand vs. a negatively charged one on heme nitrene formations here is opposite to that on heme carbene formations, for which a neutral ligand is more favorable.[13a] This is because the direction of the electronic driving force (the main charge transfer) in the cases of heme carbenes is reversed, i.e. it is from carbene to Fe, unlike here from Fe to nitrene. These comparison results further show the importance of using electronic driving force in understanding reactivity differences of axial ligands.

Hydrogen atom transfer step

For the hydrogen atom transfer step in the C–H amination reaction, i.e. from the nitrene intermediate (**Int2**) to **TS2**, as shown in Figure 2E–H, the most significant CT happens from the remaining part of the nitrene to N, Q_{CT2}, for all four ligand cases, to accompany the hydrogen atom transfer to this N. It is also negative as for Q_{CT1}. The Q_{CT2} values of around 0.2 e are smaller than those in the nitrene formation step (Q_{CT1} ~0.3 e, Table 1),which is consistent with the fact that the overall RDS is the latter. It is interesting to note that $|Q_{CT2}|$ follows a trend of $MeO^- < SH^- < MeOH <$ None, same as the reaction barrier trend of this step, suggesting an effect of the axial ligand on CT to affect reactivity in this step. However, this $|Q_{CT2}|$ trend is opposite to that for $|Q_{CT1}|$. This is because the CT direction for **TS2** is toward the axial ligand, while that for **TS1** is away from it. As a result, the stronger charge donation axial ligand (such as MeO^-) will counter this CT at **TS2** to make it smaller, as observed here.

Another significant electronic feature of **TS2** is the partial formation of the carbon radical at the benzylic position due to partial hydrogen atom transfer, as evident by its ~0.5 e spin

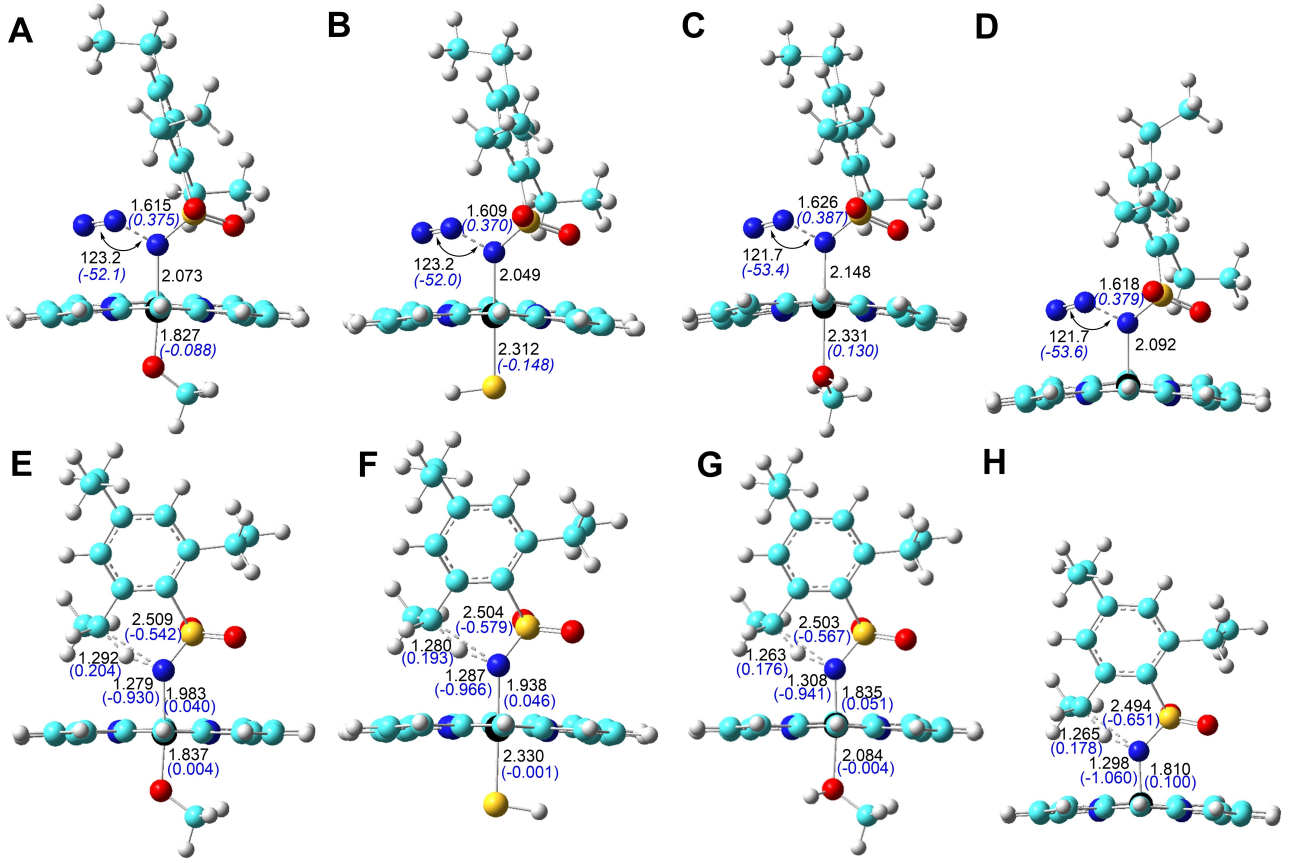

Figure 3. Key geometric parameters (in black) and changes (in blue) at **TS1** (**A**–**D**) with respect to reactants and **TS2** (**E**–**H**) with respect to **Int2** for the four axial ligand cases. Atom color scheme: Fe, black; O, red; C, cyan; H, gray; S, yellow; N, blue.

density, see Table 1. It has a trend of MeO^-(0.525 e) > SH^- (0.515 e) > MeOH (0.499 e) ~ None (0.498 e), which is opposite to the barrier trend and thus indicates that a more complete radical transfer is associated with a lower barrier. As illustrated in Figure 4A for the axial ligand MeO^-, initially **Int2** has nitrene's spin density mostly on N (~0.9 e). Then it was almost equally shared between this N (0.526 e) and the benzylic C (0.525 e) at **TS2** (Figure 4B), indicating a concerted transfer of proton and electron as a hydrogen atom. It also shows that among the two paired electrons in the original covalent benzylic C–H bond, the one goes with the transferred hydrogen has the opposite spin direction with respect to that of N, while the one remains with C has the same spin direction. As such, after the hydrogen atom is completely transferred to N, there is almost no spin density left for N (0.015 e), while the benzylic C maintains the most spin density (0.757 e) with a few shared by the neighboring phenyl ring, see Figure 4C.

In this step, the major energy cost is the partial breaking of the benzylic C–H bond for the hydrogen atom transfer. $\Delta R_{C\text{-}H}$ values in Table 1 again follow the same trend of MeO^- > SH^- > MeOH ~ None. These data suggest that **TS2** is a late transition state, as large structural changes are associated with small barriers. It should be noted that this step is a radical transfer reaction, so a partial CT would reduce the radical feature and thus affect the radical transfer efficiency. Interestingly, the $\rho^{\alpha\beta}_C$

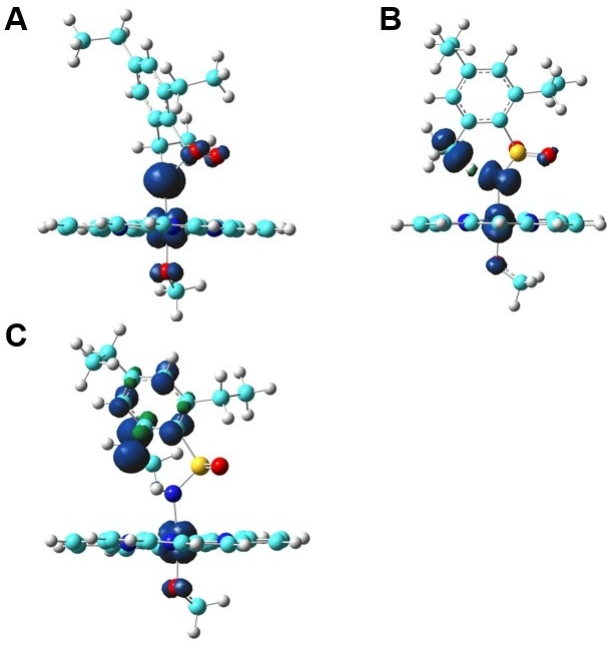

Figure 4. Spin density pictures for **Int2** (**A**), **TS2** (**B**) and **Int3** (**C**) with L = MeO^- (contour value = 0.008 au).

trend is indeed contrary to the $|Q_{CT2}|$ trend as discussed above, i.e. more radical formation is associated smaller CT amount and lower barrier in this step. Therefore, the beneficial effect of using a negatively charged ligand vs. a neutral one in this step is due to its stronger charge donation capability to counter and minimize CT for a better radical transfer reactivity.

Conclusion

Overall, this work revealed the complete reaction pathway and axial ligand effect for heme protein catalyzed intramolecular C–H aminations. Results provides the first computational support and understanding of the experimentally found RDS and relatively more favorable effect of Ser vs. Cys as axial ligand on these reactions. More importantly, the electronic origins of the axial ligand effect on both RDS (nitrene formation) and non-RDS (nitrene transfer) transition states were elucidated: the more favorable charge donation of an axial ligand facilitates the CT needed for releasing N_2 to form nitrene, while it reduces the CT occurred at the hydrogen atom transfer step to aid a more complete radical transfer feature. Both effects lead to the same reactivity trend: the barrier height trend is $MeO^- < SH^- < MeOH <$ None, where the lower barrier height gives greater reactivity. These results highlight the importance of the electronic driving forces in these steps and suggest additional venues to help future heme-based biocatalyst design in the field of sustainable C–H amination, such as 1) using an axial ligand with stronger charge donation effect than Ser; 2) removing or reducing hydrogen bonds to axial Ser (since such hydrogen bonds in the experimental system[5f,17] make the actual axial ligand environment between MeO^- and MeOH and thus less closer to the favorable pure negatively charged ligand); 3) adding electron-donating substituents on porphyrin to facilitate the beneficial CT effects as revealed from this work. Certainly, further studies to include specific protein environments and side reactions[17] will provide a more comprehensive evaluation for biocatalyst design.

Computational Methods

All calculations were performed using the program Gaussian 09.[18] All models investigated in this work were subject to full geometry optimizations without any symmetry constraints using the PCM method[19] with a dielectric constant of 4.0 to simulate the protein environment effect as done previously.[20] The frequency analysis was used to verify the nature of the stationary points on respective potential energy surfaces and to provide zero-point energy corrected electronic energies (E_{ZPE}'s), enthalpies (H's), and Gibbs free energies (G's) at 1 atm and room temperature. The atomic charges and spin densities reported here are from the Natural Population Analysis (NPA) and Mulliken schemes respectively, as implemented in Gaussian 09. All structures were optimized using a range-separated hybrid DFT method with dispersion correction ωb97xd[21] with the basis set including the effective core potential (ECP) basis LanL2DZ[22] for iron and 6–311G(d) for all other atoms, based on its excellent performance in studies of related heme carbene reactions.[13,14b,d,16] The use of a much larger 6-311++G(2d,2p) basis for all non-metal atoms was found to yield similar energy results for heme reactions[13b] and thus further support the efficient use of the current basis set here. The Fe basis here was also used in most previous computational work of heme C–H aminations.[5j,11a,c,d] The connections among the transition states with the species before and after them in the reaction pathway were confirmed via intrinsic reaction coordinate calculations in Gaussian 09. To evaluate if the actual heme substituents in the real proteins could affect the conclusions from the results using non-substituted porphyrins as found in certain substituted porphyrins,[23] additional calculations using the full heme substituents were done using the same approach as in our recent computational work which reproduced heme protein catalyzed reaction stereoselectivities within 1% error.[24]

Acknowledgements

This work was supported by NSF grants CHE-1300912 and CHE-2054897 to YZ.

Conflict of Interest

The authors declare no conflict of interest.

Data Availability Statement

The data that support the findings of this study are available in the supplementary material of this article.

Keywords: amination · biocatalysis · density functional calculations · heme proteins · reaction mechanism

[1] a) M. Feng, B. Tang, S. H. Liang, X. Jiang, *Curr. Top. Med. Chem.* **2016**, *16*, 1200–1216; b) E. T. Newcomb, P. C. Knutson, B. A. Pedersen, E. M. Ferreira, *J. Am. Chem. Soc.* **2016**, *138*, 108–111; c) S. Diethelm, E. M. Carreira, *J. Am. Chem. Soc.* **2013**, *135*, 8500–8503; d) E. Vitaku, D. T. Smith, J. T. Njardarson, *J. Med. Chem.* **2014**, *57*, 10257–10274; e) C. J. A. Ribeiro, J. D. Amaral, C. M. P. Rodrigues, R. Moreira, M. M. M. Santos, *Bioorg. Med. Chem.* **2014**, *22*, 577–584.

[2] a) H. M. L. Davies, J. R. Manning, *Nature* **2008**, *451*, 417–424; b) P. Müller, C. Fruit, *Chem. Rev.* **2003**, *103*, 2905–2920; c) H. M. L. Davies, *Angew. Chem. Int. Ed.* **2006**, *45*, 6422–6425; *Angew. Chem.* **2006**, *118*, 6574–6577.

[3] a) Z. Li, D. A. Capretto, R. Rahaman, C. He, *Angew. Chem. Int. Ed.* **2007**, *46*, 5184–5186; *Angew. Chem.* **2007**, *119*, 5276–5278; b) T. M. Figg, S. Park, J. Park, S. Chang, D. G. Musaev, *Organometallics* **2014**, *33*, 4076–4085.

[4] a) C.-M. Che, V. K.-Y. Lo, C.-Y. Zhou, J.-S. Huang, *Chem. Soc. Rev.* **2011**, *40*, 1950–1975; b) R. Singh, A. Mukherjee, *ACS Catal.* **2019**, *9*, 3604–3617; c) R. K. Zhang, X. Huang, F. H. Arnold, *Curr. Opin. Chem. Biol.* **2019**, *49*, 67–75.

[5] a) J. A. McIntosh, P. S. Coelho, C. C. Farwell, Z. J. Wang, J. C. Lewis, T. R. Brown, F. H. Arnold, *Angew. Chem. Int. Ed.* **2013**, *52*, 9309–9312; *Angew. Chem.* **2013**, *125*, 9479–9482; b) M. Bordeaux, R. Singh, R. Fasan, *Bioorg. Med. Chem.* **2014**, *22*, 5697–5704; c) R. Singh, M. Bordeaux, R. Fasan, *ACS Catal.* **2014**, *4*, 546–552; d) T. K. Hyster, C. C. Farwell, A. R. Buller, J. A. McIntosh, F. H. Arnold, *J. Am. Chem. Soc.* **2014**, *136*, 15505–15508; e) R. Singh, J. N. Kolev, P. A. Sutera, R. Fasan, *ACS Catal.* **2015**, *5*, 1685–1691; f) C. K. Prier, R. K. Zhang, A. R. Buller, S. Brinkmann-Chen, F. H. Arnold, *Nat. Chem.* **2017**, *9*, 629–634; g) E. J. Moore, R. Fasan, *Tetrahedron* **2019**, *75*, 2357–2363; h) V. Steck, J. N. Kolev, X. Ren, R. Fasan, *J. Am. Chem. Soc.* **2020**, *142*, 10343–10357; i) Z.-J. Jia, S. Gao, F. H. Arnold, *J. Am. Chem.*

Soc. **2020**, *142*, 10279–10283; j) S. V. Athavale, S. Gao, Z. Liu, S. C. Mallojjala, J. S. Hirschi, F. H. Arnold, *Angew. Chem. Int. Ed.* **2021**, *60*, 24864–24869.
[6] a) V. Lyaskovskyy, A. I. O. Suarez, H. Lu, H. Jiang, X. P. Zhang, B. de Bruin, *J. Am. Chem. Soc.* **2011**, *133*, 12264–12273; b) J. V. Ruppel, R. M. Kamble, X. P. Zhang, *Org. Lett.* **2007**, *9*, 4889–4892; c) P. F. Kuijpers, J. I. van der Vlugt, S. Schneider, B. de Bruin, *Chemistry* **2017**, *23*, 13819–13829; d) Y. Hu, K. Lang, C. Li, J. B. Gill, I. Kim, H. Lu, K. B. Fields, M. Marshall, Q. Cheng, X. Cui, L. Wojtas, X. P. Zhang, *J. Am. Chem. Soc.* **2019**, *141*, 18160–18169; e) M. Goswami, C. Rebreyend, B. De Bruin, *Molecules* **2016**, *21*, 242; f) P. F. Kuijpers, M. J. Tiekink, W. B. Breukelaar, D. L. J. Broere, N. P. van Leest, J. I. van der Vlugt, J. N. H. Reek, B. de Bruin, *Chemistry* **2017**, *23*, 7945–7952.
[7] a) X. F. Lin, C. M. Che, D. L. Phillips, *J. Org. Chem.* **2008**, *73*, 529–537; b) G. Manca, E. Gallo, D. Intrieri, C. Mealli, *ACS Catal.* **2014**, *4*, 823–832; c) Z. Guo, X. Guan, J.-S. Huang, W.-M. Tsui, Z. Lin, C.-M. Che, *Chem. Eur. J.* **2013**, *19*, 11320–11331.
[8] S. Cenini, E. Gallo, A. Caselli, F. Ragaini, S. Fantauzzi, C. Piangiolino, *Coord. Chem. Rev.* **2006**, *250*, 1234–1253.
[9] a) S. Fantauzzi, E. Gallo, A. Caselli, C. Piangiolino, F. Ragaini, S. Cenini, *Eur. J. Org. Chem.* **2007**, *2007*, 6053–6059; b) S. Bräse, C. Gil, K. Knepper, V. Zimmermann, *Angew. Chem. Int. Ed.* **2005**, *44*, 5188–5240; *Angew. Chem.* **2005**, *117*, 5320–5374; c) K. Shin, H. Kim, S. Chang, *Acc. Chem. Res.* **2015**, *48*, 1040–1052.
[10] P. Dydio, H. M. Key, H. Hayashi, D. S. Clark, J. F. Hartwig, *J. Am. Chem. Soc.* **2017**, *139*, 1750–1753.
[11] a) J. Wang, H. Gao, L. Yang, Y. Q. Gao, *ACS Catal.* **2020**, *10*, 5318–5327; b) X. Li, L. Dong, Y. Liu, *Inorg. Chem.* **2020**, *59*, 1622–1632; c) Z. Li, D. J. Burnell, R. J. Boyd, *J. Phys. Chem. B* **2017**, *121*, 10859–10868; d) S. Kalita, S. Shaik, K. D. Dubey, *Chem. Sci.* **2021**, *12*, 14507–14518.
[12] a) L. Jin, Q. Wang, X. Chen, N. Liu, X. Fang, Y.-F. Yang, Y.-B. She, *J. Org. Chem.* **2020**, *85*, 14879–14889; b) A. Prasanthi, S. Begum, H. K. Srivastava, S. K. Tiwari, R. Singh, *ACS Catal.* **2018**, *8*, 8369–8375.
[13] a) R. L. Khade, Y. Zhang, *J. Am. Chem. Soc.* **2015**, *137*, 7560–7563; b) R. L. Khade, Y. Zhang, *Chem. Eur. J.* **2017**, *23*, 17654–17658.
[14] a) K. Chen, S.-Q. Zhang, O. F. Brandenberg, X. Hong, F. H. Arnold, *J. Am. Chem. Soc.* **2018**, *140*, 16402–16407; b) Y. Wei, A. Tinoco, V. Steck, R. Fasan, Y. Zhang, *J. Am. Chem. Soc.* **2018**, *140*, 1649–1662; c) H. Su, G. Ma, Y. Liu, *Inorg. Chem.* **2018**, *57*, 11738–11745; d) R. L. Khade, A. L. Chandgude, R. Fasan, Y. Zhang, *ChemCatChem* **2019**, *11*, 3101–3108; e) R. Balhara, R. Chatterjee, G. Jindal, *Phys. Chem. Chem. Phys.* **2021**, *23*, 9500–9511; f) P. Vidossich, M. Alfonso-Prieto, C. Rovira, *J. Inorg. Biochem.* **2012**, *117*, 292–297; g) P. Rydberg, E. Sigfridsson, U. Ryde, *J. Biol. Inorg. Chem.* **2004**, *9*, 203–223; h) T. Ohta, P. Nagaraju, J.-G. Liu, T. Ogura, Y. Naruta, *J. Biol. Inorg. Chem.* **2016**, *21*, 745–755; i) S. Amanullah, A. Singha, A. Dey, *Coord. Chem. Rev.* **2019**, *386*, 183–208; j) Z. Ma, N. Nakatani, H. Fujii, M. Hada, *Phys. Chem. Chem. Phys.* **2020**, *22*, 12173–12179; k) S. P. De Visser, L. Tahsini, W. Nam, *Chem. Eur. J.* **2009**, *15*, 5577–5587.
[15] Y. Moreau, H. Chen, E. Derat, H. Hirao, C. Bolm, S. Shaik, *J. Phys. Chem. B* **2007**, *111*, 10288–10299.
[16] D. A. Vargas, R. L. Khade, Y. Zhang, R. Fasan, *Angew. Chem. Int. Ed.* **2019**, *58*, 10148–10152; *Angew. Chem.* **2019**, *131*, 10254–10258.
[17] P. S. Coehlo, Z. J. Wang, M. E. Ener, S. A. Baril, A. Kannan, F. H. Arnold, E. M. Brustad, *Nat. Chem. Biol.* **2013**, *9*, 485–487.
[18] M. J. T. Frisch, G. W.; Schlegel, H. B.; Scuseria, G. E.; Robb, M. A.; Cheeseman, J. R.; Scalmani, G.; Barone, V.; Mennucci, B.; Petersson, G. A.; Nakatsuji, H.; Caricato, M.; Li, X.; Hratchian, H. P.; Izmaylov, A. F.; Bloino, J.; Zheng, G.; Sonnenberg, J. L.; Hada, M.; Ehara, M.; Toyota, K.; Fukuda, R.; Hasegawa, J.; Ishida, M.; Nakajima, T.; Honda, Y.; Kitao, O.; Nakai, H.; Vreven, T.; Montgomery, Jr., J. A.; J. Peralta, E.; Ogliaro, F.; Bearpark, M.; Heyd, J. J.; Brothers, E.; Kudin, K. N.; Staroverov, V. N.; Keith, T.; Kobayashi, R.; Normand,J.; Raghavachari, K.; Rendell, A.; Burant, J. C.; Iyengar, S. S.; Tomasi, J.; Cossi, M.; Rega, N.; Millam, J. M.; Klene, M.; Knox, J. E.; Cross, J. B.; Bakken, V.; Adamo, C.; Jaramillo, J.; Gomperts, R.; Stratmann, R. E.; Yazyev, O.; Austin, A. J.; Cammi, R.; Pomelli, C.; Ochterski, J. W.; Martin, R. L.; Morokuma, K.; Zakrzewski,V. G.; Voth, G. A.; Salvador, P.; Dannenberg, J. J.; Dapprich, S.; Daniels, A. D.; Farkas, O.; Foresman, J. B.; Ortiz, J. V.; Cioslowski, J.; Fox, D. J.; Gaussian 09, Revision D.01 ed., Gaussian, Inc., Wallingford CT, **2013**.
[19] B. Mennucci, J. Tomasi, *J. Chem. Phys.* **1997**, *106*, 5151–5158.
[20] R. A. Torres, T. Lovell, L. Noodleman, D. A. Case, *J. Am. Chem. Soc.* **2003**, *125*, 1923–1936.
[21] J.-D. Chai, M. Head-Gordon, *Phys. Chem. Chem. Phys.* **2008**, *10*, 6615–6620.
[22] P. J. Hay, W. R. Wadt, *J. Chem. Phys.* **1985**, *82*, 270–283.
[23] E. Casali, E. Gallo, L. Toma, *Inorg. Chem.* **2020**, *59*, 11329–11336.
[24] A. Tinoco, Y. Wei, J. P. Bacik, E. J. Moore, N. Ando, Y. Zhang, R. Fasan, *ACS Catal.* **2019**, *9*, 1514–1524.

Manuscript received: June 28, 2022
Accepted manuscript online: July 15, 2022
Version of record online: August 23, 2022